

Orbit Modeling for Simultaneous Tracking and Navigation using LEO Satellite Signals

Joshua J. Morales, Joe Khalife, Ulices Santa Cruz, and Zaher M. Kassas
University of California, Irvine

BIOGRAPHIES

Joshua J. Morales is a Ph.D. Candidate in the Department of Electrical Engineering and Computer Science at the University of California, Irvine (UCI) and a member of the Autonomous Systems Perception, Intelligence, and Navigation (ASPIN) Laboratory. He received a B.S. in Electrical Engineering with High Honors from the University of California, Riverside. In 2016 he was accorded an Honorable Mention from the National Science Foundation (NSF). His research interests include estimation theory, navigation systems, autonomous vehicles, and cyber-physical systems.

Joe J. Khalife is a Ph.D. candidate in the Department of Electrical Engineering and Computer Science at UCI. He received a B.E. in Electrical Engineering and an M.S. in Computer Engineering from the Lebanese American University (LAU). From 2012 to 2015, he was a research assistant at LAU. He is a member of the ASPIN Laboratory where his research interests include opportunistic navigation, autonomous vehicles, and software-defined radio.

Ulices Santa Cruz is a Ph.D. student in the Department of Mechanical and Aerospace Engineering at UCI. He received the B.E. degree with High Honors in Mechatronics Engineering from the Universidad Autónoma de Baja California, Baja California, Mexico and the M.S. degree in Astronautics and Space Engineering from the Cranfield University, England, UK. From 2015-2017, he was a Test Engineer in the Systems Integration Laboratory at the Research and Technology Center of Honeywell Aerospace. His research interests include autonomous vehicles, navigation, satellite systems, control theory, and intelligent transportation systems.

Zaher (Zak) M. Kassas is an assistant professor at UCI and director of the ASPIN Laboratory. He received a B.E. in Electrical Engineering from the Lebanese American University, an M.S. in Electrical and Computer Engineering from The Ohio State University, and an M.S.E. in Aerospace Engineering and a Ph.D. in Electrical and Computer Engineering from The University of Texas at Austin. In 2018, he received the NSF Faculty Early Career Development Program (CAREER) award, and in 2019, he received the Office of Naval Research (ONR) Young Investigator Program (YIP) award. His research interests include cyber-physical systems, estimation theory, navigation systems, autonomous vehicles, and intelligent transportation systems.

ABSTRACT

Low Earth orbit (LEO) satellite propagation models are studied and compared for use in an extended Kalman filter (EKF)-based simultaneous tracking and navigation (STAN) framework. Three propagation models are compared: Simplified General Perturbation 4 (SGP4), two-body, and two-body with the second gravitational zonal coefficient J_2 . Each model is evaluated by studying its open-loop propagation error. The purpose of the evaluation is to select a model with small open-loop propagation error and low model complexity. The two-body with J_2 model is selected to possess a good tradeoff between propagation error and model complexity. Experimental results are presented demonstrating an unmanned aerial vehicle (UAV) flying for 160 seconds, the last 45 seconds of which are without GNSS signals. Three navigation frameworks are compared: (i) a GNSS-aided inertial navigation system (INS), and a LEO-aided INS STAN with two Orbcomm LEO satellites utilizing the two-body model (ii) without J_2 and (iii) with J_2 . It is shown that the 3-D position RMSE and final position errors with the unaided INS are 73.1 m and 162.6 m, respectively; the 3-D position RMSE and final position errors with the LEO-aided INS STAN without J_2 are 13.4 m and 26.1 m, respectively; and 3-D position RMSE and final position errors with the LEO-aided INS STAN with J_2 are 5.3 m and 5.4 m, respectively.

I. INTRODUCTION

Tens of thousands of broadband low Earth orbit (LEO) satellites are expected to be operational by the mid-2020s [1]. These planned broadband LEO satellites along with current existing communication LEO satellites will bring an

abundance of ambient radio frequency signals that may be treated as signals of opportunity (SOPs) for navigation in the inevitable event that global navigation satellite system (GNSS) signals become unavailable (e.g., in deep urban canyons and near dense foliage) or untrustworthy (e.g., during intentional and unintentional jamming and malicious spoofing attacks) [2, 3]. In the absence of GNSS signals, LEO signals could be exploited to provide aiding corrections to a vehicle’s inertial navigation system (INS).

SOPs have been considered as sources for navigation in the absence of GNSS signals [4, 5]. SOPs include AM/FM radio [6, 7], cellular [8–15], digital television [16, 17], and LEO satellites [18–23]. LEO satellites are particularly attractive aiding sources for a vehicle’s INS in GNSS-challenged environments for several reasons. LEO satellites provide an abundance of transmitted signals that are: (i) diverse in direction, which yields a low geometric dilution of precision (GDOP) [24]; (ii) centered at various frequencies, which provides independent sources of information that can be used to detect a spoofing attack; and (iii) transmitted from around twenty times closer to the Earth compared to GNSS satellite signals that are transmitted from medium Earth orbit (MEO), making them received 300 to 2400 times more powerful than GNSS signals [25].

To exploit LEO satellite signals for navigation, their states (positions and clock errors) must be known. LEO satellites have been exploited as sources of navigation when their states were assumed to be known [26]. However, unlike GNSS satellites that periodically transmit accurate information about their positions and clock errors, such information about LEO satellites’ states may be unavailable, in which case they must be estimated along with the vehicles’ states (orientation, position, velocity, inertial measurement unit (IMU) biases, and clock errors). This estimation problem may be cast as an extended Kalman filter (EKF)-based simultaneous tracking and navigation (STAN) problem, where signals transmitted from LEO satellites are used to simultaneously track the satellites’ and vehicle’s states [23, 27–29]. The STAN problem is similar to the radio simultaneous localization and mapping (SLAM) problem [30, 31]. However, in contrast to radio SLAM, which estimates the static terrestrial SOPs’ positions, STAN is more challenging, as one must estimate the dynamic stochastic states corresponding to the LEO satellites’ position and velocity.

The EKF-based STAN framework requires a dynamics model to propagate the state estimates and corresponding estimation uncertainties of LEO satellites. In [32], a two-body orbit model was used to propagate the LEO satellites’ position and velocity states. However, it is known that the two-body orbit model quickly accumulates error between measurement epochs. This accumulation of position and velocity error degrades the navigation performance. While orbit propagation models have been studied for several decades for long-term orbit propagation, this work studies orbit models for STAN, which is interested in short-term orbit propagation performance of LEO satellites. Specifically, this paper studies and compares three different dynamic models for propagation in the STAN framework: (i) Simplified Generalize Perturbation 4 (SGP4), (ii) two-body, and (iii) two-body with J_2 . The purpose of this study is to select a model that produces small short-term open-loop propagation errors and remains computationally efficient, so that broadband LEO satellites may be propagated in the STAN framework in real-time.

The remainder of this paper is organized as follows. Section II describes the STAN framework and discusses the receiver dynamics and measurement models. Section III discusses and compares three LEO satellite dynamics models. Section IV presents experimental results demonstrating an unmanned aerial vehicle (UAV) navigating with Orbcomm signals using the LEO satellite signal-aided INS framework. Concluding remarks are given in Section V.

II. STAN FRAMEWORK

The STAN framework employs an EKF to aid an INS with LEO satellite pseudorange rates and GNSS pseudoranges, when available, in a tightly-coupled fashion. This framework, illustrated in Fig. 1 (a), works similarly to that of a traditional tightly-coupled GNSS-aided INS [33] with two main differences: (i) the position and clock states of the LEO satellites are unknown to the receiver; hence, they are estimated along with the states of the navigating vehicle and (ii) Doppler measurements are used to aid the INS instead of GNSS pseudoranges. The EKF-based STAN framework requires a LEO satellite propagation model to propagate the LEO satellites’ position and velocity and their corresponding estimation uncertainties between measurement epochs. This work compares the four LEO propagation models listed in Fig. 1 (b) for use in a STAN framework. The state vector to be estimated and the measurement models are described next.

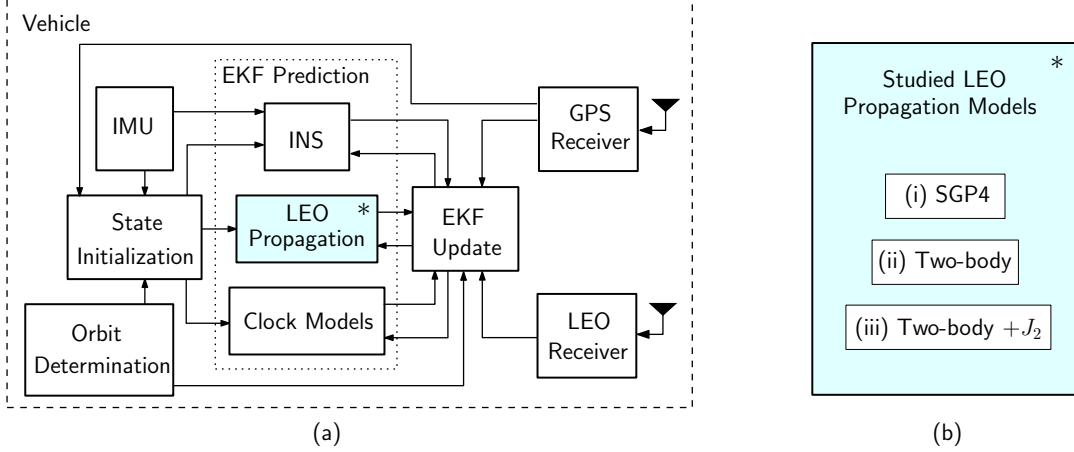


Fig. 1. (a) Tightly-coupled LEO-aided INS navigation framework and (b) LEO propagation models studied in this paper.

A. State Model

The EKF state vector is given by

$$\mathbf{x} = [\mathbf{x}_r^\top, \mathbf{x}_{\text{leo}_1}^\top, \dots, \mathbf{x}_{\text{leo}_M}^\top]^\top,$$

$$\mathbf{x}_r = \left[\frac{B}{G}\bar{\mathbf{q}}^\top, \mathbf{r}_r^\top, \dot{\mathbf{r}}_r^\top, \mathbf{b}_g^\top, \mathbf{b}_a^\top, c\delta t_r, c\dot{\delta}t_r \right]^\top, \quad \mathbf{x}_{\text{leo}_m} = \left[\mathbf{r}_{\text{leo}_m}^\top, \dot{\mathbf{r}}_{\text{leo}_m}^\top, c\delta t_{\text{leo}_m}, c\dot{\delta}t_{\text{leo}_m} \right]^\top,$$

where \mathbf{x}_r is the state vector of the vehicle-mounted IMU and receiver which consists of $\frac{B}{G}\bar{\mathbf{q}}$, which is a four-dimensional (4-D) unit quaternion representing the orientation of a body frame B fixed at the IMU with respect to a global frame G , \mathbf{r}_r and $\dot{\mathbf{r}}_r$ are the three-dimensional (3-D) position and velocity of the IMU, \mathbf{b}_g and \mathbf{b}_a are 3-D biases of the IMU's gyroscopes and accelerometers, respectively, δt_r and $\dot{\delta}t_r$ are the clock bias and drift of the receiver, respectively, and c is the speed of light. The vector $\mathbf{x}_{\text{leo}_m}$ is composed of the states of the m^{th} LEO satellite: $\mathbf{r}_{\text{leo}_m}$ and $\dot{\mathbf{r}}_{\text{leo}_m}$ are the 3-D satellite position and velocity, respectively, δt_{leo_m} and $\dot{\delta}t_{\text{leo}_m}$ are the satellite's transceiver clock bias and drift, respectively, $m = 1, \dots, M$, with M being the total number of LEO satellites visible to the receiver.

The EKF propagates an estimate of the vehicle's orientation, position, and velocity in time using IMU data, which is processed through standard INS kinematic equations [34]. The accelerometer and gyroscope biases are propagated using a velocity random walk model. The clock states of both the vehicle and the LEO satellites are propagated using a double integrator model driven by process noise [35]. The LEO satellite position and velocity propagation models will be discussed and compared in Section III.

B. LEO Satellite Receiver Doppler Measurement Model

The vehicle-mounted LEO satellite signal receiver makes Doppler frequency measurements f_D on the available LEO satellite signals, from which a pseudorange rate measurement $\dot{\rho}$ can be obtained from $\dot{\rho} = -\frac{c}{f_c}f_D$, where f_c is the carrier frequency. The pseudorange rate measurement $\dot{\rho}_m$ at the k^{th} time-step from the m^{th} LEO satellite is modeled according to

$$\dot{\rho}_m(k) = [\dot{\mathbf{r}}_{\text{leo}_m}(k) - \dot{\mathbf{r}}_r(k)]^\top \frac{[\mathbf{r}_r(k) - \mathbf{r}_{\text{leo}_m}(k)]}{\|\mathbf{r}_r(k) - \mathbf{r}_{\text{leo}_m}(k)\|_2} + c \cdot [\dot{\delta}t_r(k) - \dot{\delta}t_{\text{leo}_m}(k)] + c\dot{\delta}t_{\text{iono}_m}(k) + c\dot{\delta}t_{\text{trop}_m}(k) + v_{\dot{\rho}_m}(k),$$

where $\dot{\delta}t_{\text{iono}_m}$ and $\dot{\delta}t_{\text{trop}_m}$ are the drifts of the ionospheric and tropospheric delays, respectively, for the m^{th} LEO satellite and $v_{\dot{\rho}_m}$ is the measurement noise, which is modeled as a white Gaussian random sequence with variance $\sigma_{v_{\dot{\rho}_m}}^2$. Note that the variation in the ionospheric and tropospheric delays during LEO satellite visibility is negligible compared to the errors in the satellite's estimated velocities [36]; hence, $\dot{\delta}t_{\text{iono}_m}$ and $\dot{\delta}t_{\text{trop}_m}$ are ignored in the measurement model, yielding the measurement model given by

$$\dot{\rho}_m(k) \approx [\dot{\mathbf{r}}_{\text{leo}_m}(k) - \dot{\mathbf{r}}_r(k)]^\top \frac{[\mathbf{r}_r(k) - \mathbf{r}_{\text{leo}_m}(k)]}{\|\mathbf{r}_r(k) - \mathbf{r}_{\text{leo}_m}(k)\|_2} + c \cdot [\dot{\delta}t_r(k) - \dot{\delta}t_{\text{leo}_m}(k)] + v_{\dot{\rho}_m}(k). \quad (1)$$

III. LEO SATELLITE DYNAMIC MODEL ANALYSIS

In this section, the three LEO position and velocity propagation models listed in Fig. 1 (b) are analyzed for use in an EKF-based STAN framework. The goal of this analysis is to select a propagation model that (i) produces small position error after several minutes of open-loop propagation, (ii) be implementable in an EKF (analytically linearizable), and (iii) remain computationally efficient so that many LEO satellites can simultaneously be propagated in the STAN framework in real-time.

A. Propagation Model Test Setup

Each propagation model is analyzed by comparing the propagated LEO satellite position and velocity with real GPS-derived position and velocity data, which is transmitted from Orbcomm satellite-mounted GPS receivers every four seconds. The Orbcomm constellation is a wide area two-way communication system that uses a constellation of LEO satellites to provide worldwide geographic coverage for sending and receiving alphanumeric packets [37]. Orbcomm satellites reside in an altitude ranging from 740 km to 975 km. Two different Orbcomm satellites are used over approximately 450 seconds to analyze each propagation model. The SGP4 model is analyzed by computing the error between the GPS receiver’s position and velocity and the corresponding position and velocity produced by SGP4. The remaining two models are studied using a Monte Carlo-type analysis according to the following procedure:

1. Collect K Orbcomm LEO satellite-mounted GPS receiver positions $\mathbf{r}_{\text{leo}}(k)$ and velocities $\dot{\mathbf{r}}_{\text{leo}}(k)$, where $k = 1, 2, \dots, K$, at 4 second intervals from two satellites.
2. Set a counter $j \equiv 1$.
3. The candidate propagator is initialized using $\mathbf{r}_{\text{leo}}(j)$ and $\dot{\mathbf{r}}_{\text{leo}}(j)$. Denote these initial estimates as $\hat{\mathbf{r}}_{\text{leo}}(j)$ and $\hat{\dot{\mathbf{r}}}_{\text{leo}}(j)$, respectively.
4. The candidate propagator propagates the position $\hat{\mathbf{r}}_{\text{leo}}(j)$ and velocity $\hat{\dot{\mathbf{r}}}_{\text{leo}}(j)$ to $\hat{\mathbf{r}}_{\text{leo}}(k)$ and $\hat{\dot{\mathbf{r}}}_{\text{leo}}(k)$, respectively, where $k = j + 1, j + 2, \dots, K$.
5. The error between the GPS receiver’s position and the propagated one is computed according to $\|\mathbf{r}_{\text{leo}}(k) - \hat{\mathbf{r}}_{\text{leo}}(k)\|_2$, where $k = j + 1, j + 2, \dots, K$.
6. Increment j and loop back to step 3 until $j = K$.

The next two subsections discuss each propagator and summarize the results of the analysis.

B. SGP4 Propagation

The satellites’ Keplerian elements and perturbing acceleration parameters are contained in publicly available two-line element (TLE) file sets [38]. The information in these files may be used to initialize the SGP4 model, which is specifically designed to propagate a LEO satellite’s orbit [39]. SGP propagators are optimized for speed by replacing complicated perturbing acceleration models that require numerical integrations with analytical expressions to propagate a satellite position from an epoch time to a specified future time. The tradeoff is in satellite position accuracy—the SGP4 propagator has around 3 km in position error at epoch and the propagated orbit will continue to deviate from its true one until the TLE files are updated the following day. The position and velocity error computed according to the procedure discussed in Subsection III-A are plotted in Fig. 2 for satellite 1 and 2.

Notice from Fig. 2 that the position error is approximately 3 km at initialization time, as expected. The error for satellite 1 increases by approximately 80 meters after 450 seconds of propagation time. The error for satellite 2 decreases by approximately 80 meters. This decrease is due to the errors being periodic over short periods of time. The errors over longer propagation periods will begin to increase. The SGP4 model is determined to be unsuitable for use in the STAN framework for the following reasons. First, while the increase in error of the SGP4 model over short periods of time would be suitable for use in the STAN framework, the initial error is large. Second, the SGP4 model cannot be initialized with an externally derived position and velocity, i.e., only TLE files can be used for initialization. Third, the propagation algorithm is treated as a “gray box” propagator; therefore, it would be difficult to derive state transition matrices to propagate corresponding LEO satellite position and velocity estimation error covariances.

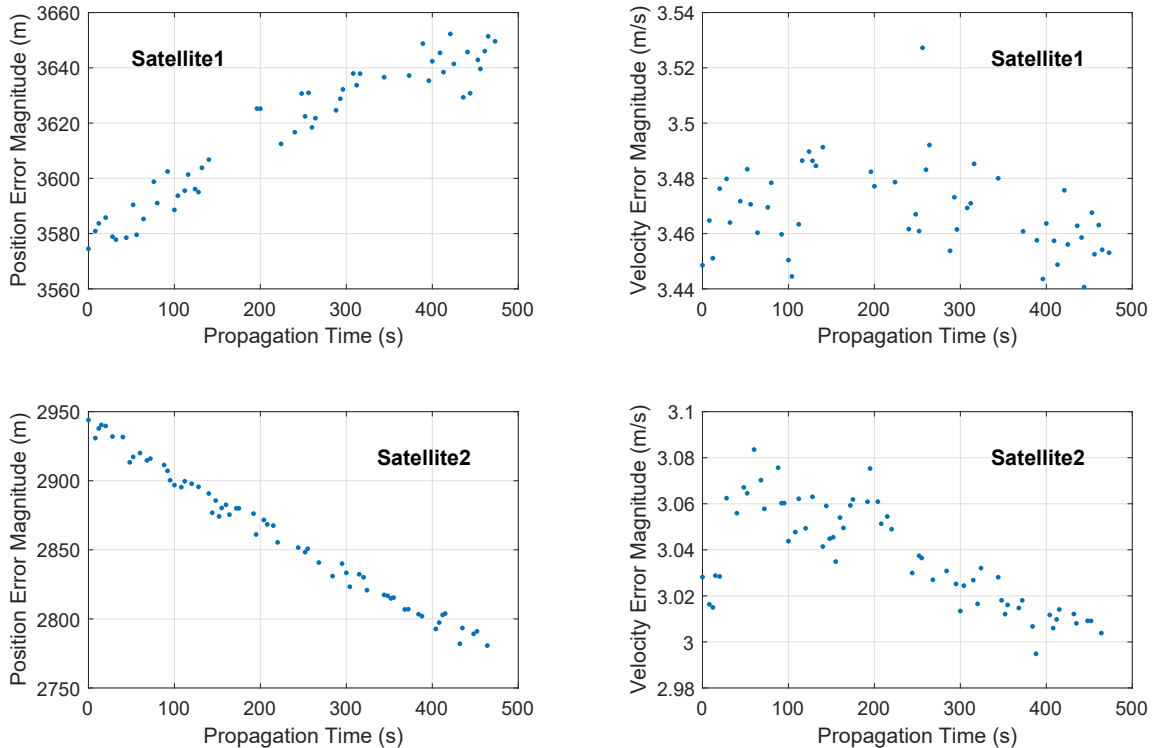


Fig. 2. SGP4 position and velocity errors for satellite 1 and satellite 2.

C. Two-Body Propagation

The two-body motion equation of the m^{th} LEO satellite is given by

$$\ddot{\mathbf{r}}_{\text{leo}_m} = -\frac{\mu}{\|\mathbf{r}_{\text{leo}_m}\|_2^3} \mathbf{r}_{\text{leo}_m} + \tilde{\mathbf{w}}_{\text{leo}_m}, \quad (2)$$

where $\ddot{\mathbf{r}}_{\text{leo}_m} = \frac{d}{dt} \dot{\mathbf{r}}_{\text{leo}_m}$, i.e., the acceleration of the m^{th} LEO satellite, μ is the standard gravitational parameter, and $\tilde{\mathbf{w}}_{\text{leo}_m}$ is process noise, which attempts to capture the overall perturbation in acceleration, which includes non-uniform Earth gravitational field, atmospheric drag, solar radiation pressure, third-body gravitational forces (e.g., gravity of the Moon and Sun), and general relativity [40]. The process noise vector $\tilde{\mathbf{w}}_{\text{leo}_m}$ is modeled as a white random vector with power spectral density (PSD) $\mathbf{Q}_{\tilde{\mathbf{w}}_{\text{leo}_m}}$.

The two-body model (2) is convenient because it has a known analytical solution; however, the perturbing accelerations are not zero mean, which this model neglects. Omitting these perturbing accelerations can cause hundreds of meters in position error after just a few minutes of open-loop propagation due to the model mismatch. The position error of the two-body propagation model computed according to the procedure discussed in Subsection III-A is plotted in Fig. 3 for satellite 1 and 2.

Note from Fig. 3 that the error magnitude of the position states for satellite 1 and 2 grows much quicker compared to the errors of the SGP4 model. While the two-body model has a known and simple analytical Jacobian for estimation error covariance propagation, the accumulation of position and velocity estimation error is large, especially for large intervals between measurement epochs. Furthermore, since the process noise vector $\tilde{\mathbf{w}}_{\text{leo}_m}$ is modeled as a white process, which is attempting to capture unmodeled perturbations, the PSD $\mathbf{Q}_{\tilde{\mathbf{w}}_{\text{leo}_m}}$ would have to be selected to over-bound these expected perturbations. This over bounding can cause a model mismatch, which can lead to incorrect propagation of the estimation error covariance, and subsequently cause inconsistent estimation or filter divergence altogether. In what follows, a more sophisticated LEO satellite dynamics model is studied, which aims to significantly reduce estimation errors by including the most significant non-zero mean perturbing acceleration components, while maintaining a simple analytical Jacobian for estimation error covariance propagation.

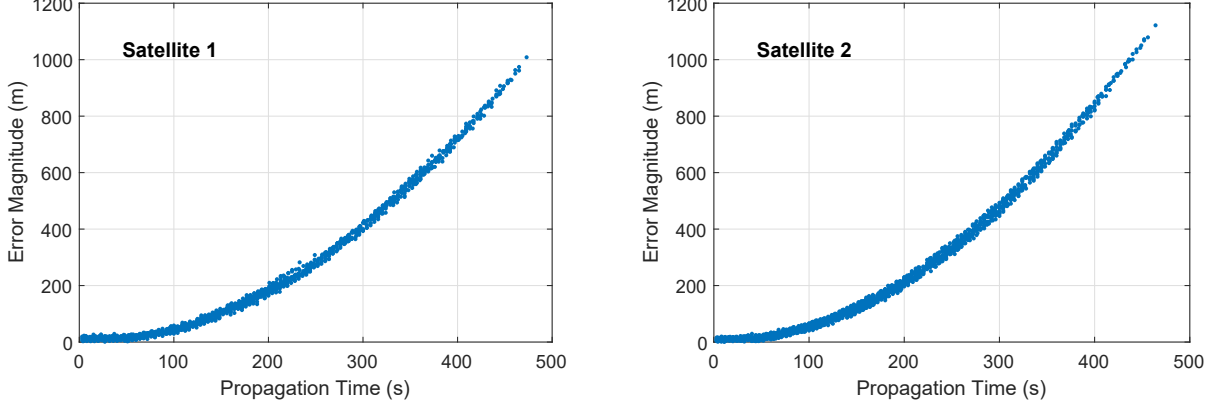


Fig. 3. Two-body position and velocity errors for satellite 1 and satellite 2.

D. Two-body with J_2

The most significant perturbing accelerations for a LEO satellite is due to Earth's non-uniform gravity \mathbf{a}_{grav} . The two-body model with \mathbf{a}_{grav} can be written more generally as

$$\ddot{\mathbf{r}}_{\text{leo}_m} = \mathbf{a}_{\text{grav}_m}, \quad \mathbf{a}_{\text{grav}_m} = \frac{dU_m}{d\mathbf{r}_{\text{leo}_m}}, \quad (3)$$

where U_m is the non-uniform gravity potential of the Earth.

To model the non-uniform gravity potential of the Earth U_m , several models have been developed. For a satellite requiring accuracies of a few meters, the JGM-3 model developed by Goddard Space Flight Center is usually sufficient [41]. In this work, the tesseral and sectoral terms of the JGM-3 model are neglected, since they are several orders of magnitude smaller than the zonal terms (denoted $\{J_n\}_{n=2}^{\infty}$). This gives the gravitational potential of the Earth at the m^{th} LEO satellite as [42]

$$U_m = \frac{\mu}{\|\mathbf{r}_{\text{leo}_m}\|} \left[1 - \sum_{n=2}^N J_n \frac{R_E^n}{\|\mathbf{r}_{\text{leo}_m}\|^n} P_n(\sin(\theta)) \right], \quad (4)$$

where P_n is a Legendre polynomial with harmonic n , J_n is the n^{th} zonal coefficient, R_E is the mean radius of the Earth, $\sin(\theta) = z_{\text{leo}_m} / \|\mathbf{r}_{\text{leo}_m}\|$, $\mathbf{r}_{\text{leo}_m} \triangleq [x_{\text{leo}_m}, y_{\text{leo}_m}, z_{\text{leo}_m}]^T$ are the position coordinates of the m^{th} LEO satellite in an Earth-centered inertial frame, and $N = \infty$. The terms of acceleration corresponding to coefficients $> J_2$ are approximately three orders of magnitude smaller than the ones due to J_2 . Therefore, the perturbation due to non-uniform gravity will be approximated by using only the term corresponding to J_2 . Taking the partial derivative of (4) with respect to the components of $\mathbf{r}_{\text{leo}_m}$ with $N \equiv 2$ gives the components of $\mathbf{a}_{\text{grav}_m} = [\ddot{x}_{\text{grav}_m}, \ddot{y}_{\text{grav}_m}, \ddot{z}_{\text{grav}_m}]^T$ to be

$$\begin{aligned} \ddot{x}_{\text{grav}_m} &= -\frac{\mu x_{\text{leo}_m}}{\|\mathbf{r}_{\text{leo}_m}\|^3} \left[1 + J_2 \frac{3}{2} \left(\frac{R_e}{\|\mathbf{r}_{\text{leo}_m}\|} \right)^2 \left(1 - 5 \frac{z_{\text{leo}_m}^2}{\|\mathbf{r}_{\text{leo}_m}\|^2} \right) \right], \\ \ddot{y}_{\text{grav}_m} &= -\frac{\mu y_{\text{leo}_m}}{\|\mathbf{r}_{\text{leo}_m}\|^3} \left[1 + J_2 \frac{3}{2} \left(\frac{R_e}{\|\mathbf{r}_{\text{leo}_m}\|} \right)^2 \left(1 - 5 \frac{z_{\text{leo}_m}^2}{\|\mathbf{r}_{\text{leo}_m}\|^2} \right) \right], \\ \ddot{z}_{\text{grav}_m} &= -\frac{\mu z_{\text{leo}_m}}{\|\mathbf{r}_{\text{leo}_m}\|^3} \left[1 + J_2 \frac{3}{2} \left(\frac{R_e}{\|\mathbf{r}_{\text{leo}_m}\|} \right)^2 \left(3 - 5 \frac{z_{\text{leo}_m}^2}{\|\mathbf{r}_{\text{leo}_m}\|^2} \right) \right]. \end{aligned} \quad (5)$$

The equations in (5) are substituted into (3), with the JGM-3 model's dimensionless zonal coefficient $J_2 = 1.08262668355 \times 10^{-2}$, and two Orbcomm LEO satellite positions were propagated. The position error was computed according to the procedure discussed in Subsection III-A. The results are plotted in Fig. 4 for satellite 1 and 2.

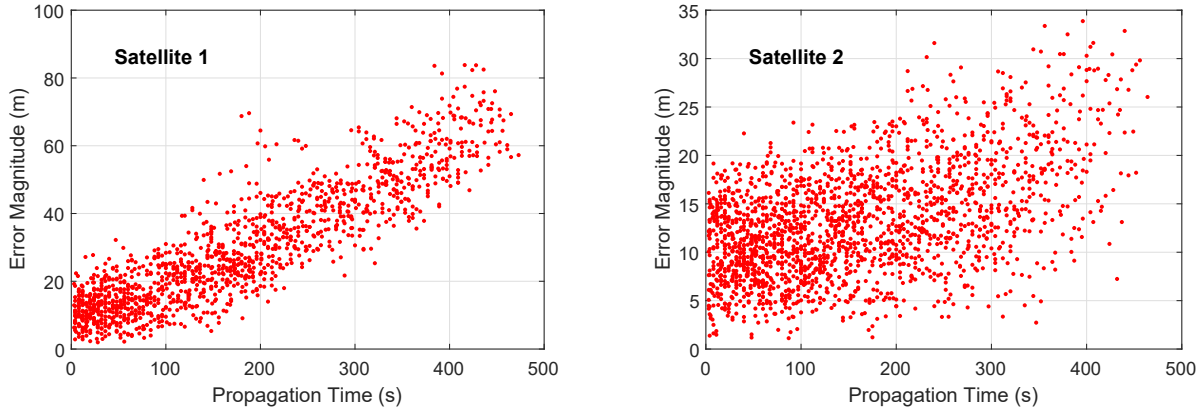


Fig. 4. Two-body with J_2 model position errors for satellite 1 and satellite 2.

The following may be concluded from the plots in Fig. 4. First, the position error grows significantly slower compared to the two-body only errors in Fig. 3. Second, the growth in error is comparable to that of the SGP4 propagation errors in Fig. 2, however; in contrast to the SGP4 propagator, the two-body with J_2 can be initialize using any *a priori* knowledge of the position and velocity of the satellite. Similar values were noted when this model was used to propagate the orbits of other Orbcomm satellites. Note that this model has desirable error characteristics for use in the STAN framework, and in contrast to the SGP4 propagator, it as has a simple and known analytical expression for the Jacobian of (3). For these reasons, the model (3) is selected as the LEO satellite propagation model for use in the STAN framework.

IV. EXPERIMENTAL RESULTS

In this section, the LEO signal-aided INS framework is demonstrated experimentally on a UAV. The experimental setup is first described and then experimental results are provided.

A. Experimental Setup

An experimental test was conducted to evaluate the performance of the proposed LEO signal-aided INS framework. To this end, a DJI Matrice 600 UAV was equipped with following hardware and software:

- A high-end quadrifilar helix antenna.
- An Ettus E312 universal software radio peripheral to sample Orbcomm signals and store the in-phase and quadrature components. These samples were then processed by the Multi-channel Adaptive TRANsceiver Information eXtractor (MATRIX) software-defined quadrature phase-shift keying (QPSK) receiver developed by the Autonomous Systems Perception, Intelligence, and Navigation (ASPIN) Laboratory to perform carrier synchronization and extract pseudorange rate observables [43].
- A consumer-grade micro-electromechanical (MEMS) IMU, which is proprietary DJI hardware used in their A3 flight controller. Log files were downloaded from the UAV to parse the raw IMU data, which were subsequently fed to the INS of the STAN framework.
- A pressure altimeter, which is proprietary DJI hardware used in their A3 flight controller. Log files were downloaded from the UAV to parse the altitude measurements, which were subsequently fed to the EKF update of the STAN framework.

The ground truth trajectory was taken from the UAV's onboard navigation system, which consists of a MEMS IMU, a multi-constellation GNSS receiver (GPS and GLONASS), a pressure altimeter, and a magnetometer. The experimental setup is shown in Fig. 5.

B. Results

The UAV flew a commanded trajectory in Irvine, California, USA, over a 160-second period during which 2 Orbcomm LEO satellites were available. Three estimators were implemented to estimate the flown trajectories: (i) the LEO

signal-aided INS STAN framework described in Section II with the two-body model excluding J_2 for LEO satellite state propagation, (ii) the LEO signal-aided INS STAN framework described in Section II with the two-body model including J_2 for LEO satellite state propagation, and (iii) a traditional GPS-aided INS for comparative analysis. All estimated trajectories were compared with the trajectory taken from the UAV's onboard navigation system.

Each estimator had access to GPS for only the first 125 seconds of the run, after which GPS signals were cut off for the remaining 45 seconds, as illustrated in Fig. 6 (d). Fig. 6 (a) shows the trajectory of the 2 Orbcomm LEO satellites traversed over the course of the experiment. The position and velocity estimates of these satellites were initialized using position and velocity data that is transmitted down from Orbcomm satellite-mounted GPS receivers. The navigating vehicle's 3-D position root mean-squared error (RMSE) of the traditional GPS-aided INS's navigation solution after GPS was cut off was 73.1 meters with a final error of 162.6 meters. The 3-D position RMSE of the UAV's trajectory for the LEO signal-aided INS with two-body model excluding J_2 was 13.4 meters with a final error of 26.1 meters. The 3-D position RMSE of the UAV's trajectory for the LEO signal-aided INS with two-body model including J_2 was 5.3 meters with a final error of 5.4 meters. The navigation results are summarized in Table I.

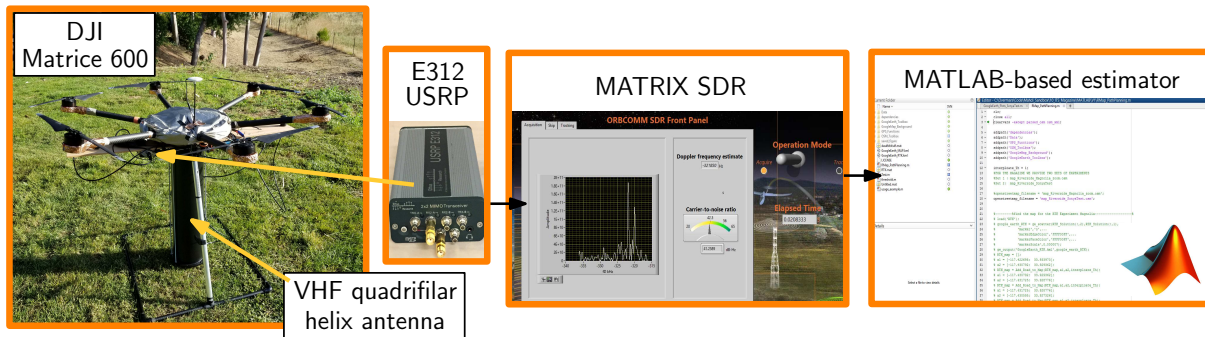


Fig. 5. Experimental setup.

TABLE I
UAV NAVIGATION PERFORMANCE

Performance Measure	INS only	STAN: two-body	STAN: two-body + J_2
RMSE (m)	73.1	13.4	5.3
Final Error (m)	162.6	26.1	5.4

V. CONCLUSIONS

This work studied three LEO satellite propagation models for use in an EKF-based STAN framework. It was found that a two-body with J_2 model provides significantly smaller satellite propagation errors compared to a two-body only model while maintaining a simple analytical expression for the dynamics Jacobian. Experimental results were presented for a UAV navigating for 160 seconds, the last 45 seconds of which were without GNSS signals. Three navigation frameworks were compared: (i) a GNSS-aided inertial navigation system (INS), and a LEO-aided INS STAN with two Orbcomm LEO satellites utilizing the two-body model (ii) without J_2 and (iii) with J_2 . It was shown that the 3-D position RMSE and final position errors with the unaided INS were 73.1 m and 162.6 m, respectively; the 3-D position RMSE and final position errors with the LEO-aided INS STAN without J_2 were 13.4 m and 26.1 m, respectively; and 3-D position RMSE and final position errors with the LEO-aided INS STAN with J_2 were 5.3 m and 5.4 m, respectively.

Acknowledgment

This work was supported in part by the Office of Naval Research (ONR) under Grant N00014-19-1-2511 and in part by the National Science Foundation (NSF) under Grant 1929965.

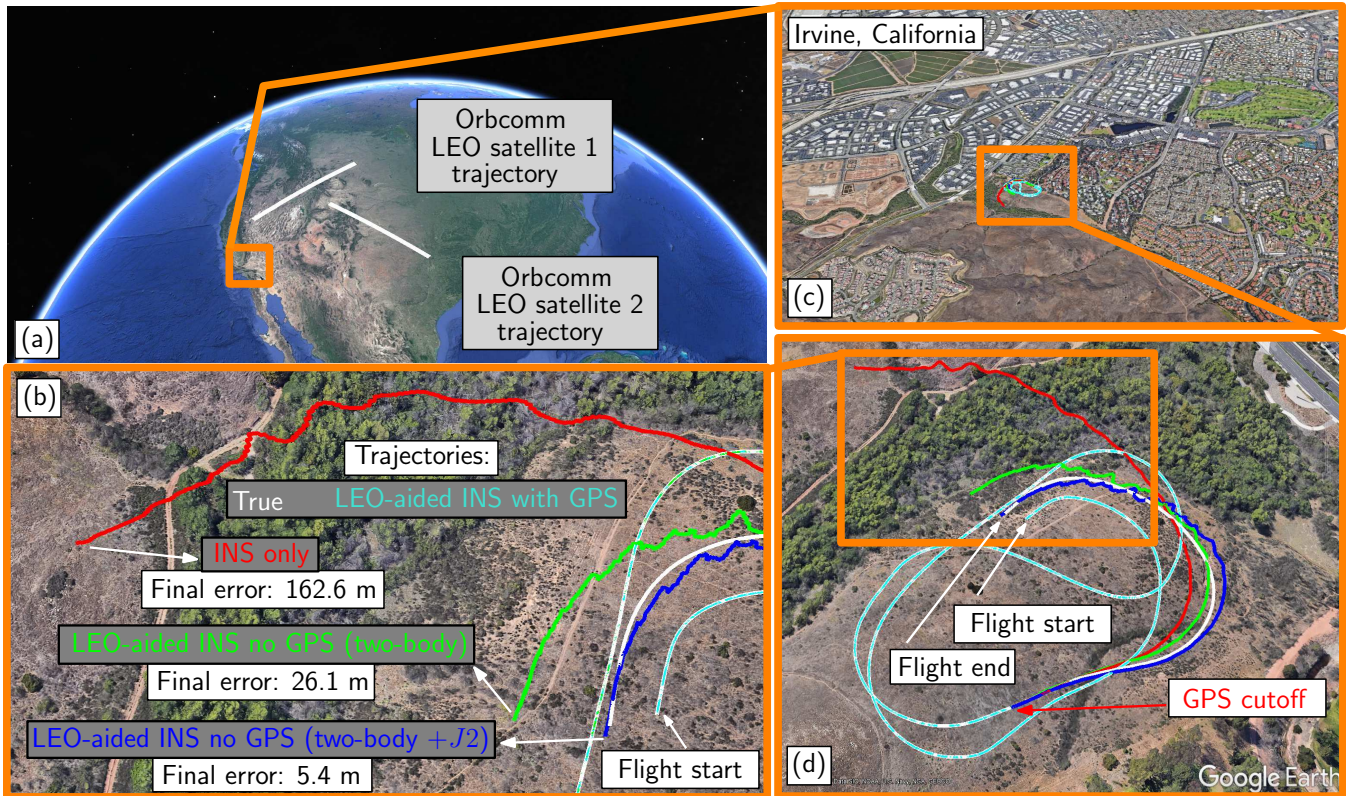


Fig. 6. Experimental results showing (a) the trajectory of the 2 Orbcomm LEO satellites, (b) zoom on the UAV's final position and final position estimates, and (c)–(d) true and estimated trajectories of the UAV.

References

- [1] The Verge, "FCC approves SpaceX's plan to launch more than 7,000 internet-beaming satellites," <https://www.theverge.com/2018/11/15/18096943/spacex-fcc-starlink-satellites-approval-constellation-internet-from-space>, November 2018, accessed October 2, 2019.
- [2] N. Kbayer and M. Sahnoudi, "Performances analysis of GNSS NLOS bias correction in urban environment using a three-dimensional city model and GNSS simulator," *IEEE Transactions on Aerospace and Electronic Systems*, vol. 54, no. 4, pp. 1799–1814, February 2018.
- [3] R. Ioannides, T. Pany, and G. Gibbons, "Known vulnerabilities of global navigation satellite systems, status, and potential mitigation techniques," *Proceedings of the IEEE*, vol. 104, no. 6, February 2016.
- [4] L. Merry, R. Faragher, and S. Schedin, "Comparison of opportunistic signals for localisation," in *Proceedings of IFAC Symposium on Intelligent Autonomous Vehicles*, September 2010, pp. 109–114.
- [5] Z. Kassas, "Collaborative opportunistic navigation," *IEEE Aerospace and Electronic Systems Magazine*, vol. 28, no. 6, pp. 38–41, 2013.
- [6] J. McEllroy, "Navigation using signals of opportunity in the AM transmission band," Master's thesis, Air Force Institute of Technology, Wright-Patterson Air Force Base, Ohio, USA, 2006.
- [7] S. Fang, J. Chen, H. Huang, and T. Lin, "Is FM a RF-based positioning solution in a metropolitan-scale environment? A probabilistic approach with radio measurements analysis," *IEEE Transactions on Broadcasting*, vol. 55, no. 3, pp. 577–588, September 2009.
- [8] C. Yang, T. Nguyen, and E. Blasch, "Mobile positioning via fusion of mixed signals of opportunity," *IEEE Aerospace and Electronic Systems Magazine*, vol. 29, no. 4, pp. 34–46, April 2014.
- [9] J. Khalife and Z. Kassas, "Navigation with cellular CDMA signals – part II: Performance analysis and experimental results," *IEEE Transactions on Signal Processing*, vol. 66, no. 8, pp. 2204–2218, April 2018.
- [10] M. Ulmschneider and C. Gentner, "Multipath assisted positioning for pedestrians using LTE signals," in *Proceedings of IEEE/ION Position, Location, and Navigation Symposium*, April 2016, pp. 386–392.
- [11] P. Müller, J. A. del Peral-Rosado, R. Piché, and G. Seco-Granados, "Statistical trilateration with skew-t distributed errors in LTE networks," *IEEE Transactions on Wireless Communications*, vol. 15, no. 10, October 2016.
- [12] Z. Kassas, J. Morales, K. Shamaei, and J. Khalife, "LTE steers UAV," *GPS World Magazine*, vol. 28, no. 4, pp. 18–25, April 2017.
- [13] Z. Kassas, J. Khalife, K. Shamaei, and J. Morales, "I hear, therefore I know where I am: Compensating for GNSS limitations with cellular signals," *IEEE Signal Processing Magazine*, pp. 111–124, September 2017.
- [14] K. Shamaei, J. Khalife, and Z. Kassas, "Exploiting LTE signals for navigation: Theory to implementation," *IEEE Transactions on Wireless Communications*, vol. 17, no. 4, pp. 2173–2189, April 2018.
- [15] K. Shamaei and Z. Kassas, "LTE receiver design and multipath analysis for navigation in urban environments," *NAVIGATION, Journal of the Institute of Navigation*, vol. 65, no. 4, pp. 655–675, December 2018.

- [16] M. Rabinowitz and J. Spilker, Jr., "A new positioning system using television synchronization signals," *IEEE Transactions on Broadcasting*, vol. 51, no. 1, pp. 51–61, March 2005.
- [17] P. Thevenon, S. Damien, O. Julien, C. Macabiau, M. Bousquet, L. Ries, and S. Corazza, "Positioning using mobile TV based on the DVB-SH standard," *NAVIGATION, Journal of the Institute of Navigation*, vol. 58, no. 2, pp. 71–90, 2011.
- [18] M. Rabinowitz, B. Parkinson, C. Cohen, M. O'Connor, and D. Lawrence, "A system using LEO telecommunication satellites for rapid acquisition of integer cycle ambiguities," in *Proceedings of IEEE/ION Position Location and Navigation Symposium*, April 1998, pp. 137–145.
- [19] M. Joerger, L. Gratton, B. Pervan, and C. Cohen, "Analysis of Iridium-augmented GPS for floating carrier phase positioning," *NAVIGATION, Journal of the Institute of Navigation*, vol. 57, no. 2, pp. 137–160, 2010.
- [20] K. Pesyna, Z. Kassas, and T. Humphreys, "Constructing a continuous phase time history from TDMA signals for opportunistic navigation," in *Proceedings of IEEE/ION Position Location and Navigation Symposium*, April 2012, pp. 1209–1220.
- [21] T. Reid, A. Neish, T. Walter, and P. Enge, "Leveraging commercial broadband LEO constellations for navigating," in *Proceedings of ION GNSS Conference*, September 2016, pp. 2300–2314.
- [22] R. Landry, A. Nguyen, H. Rasaea, A. Amrhar, X. Fang, and H. Benzerrouk, "Iridium Next LEO satellites as an alternative PNT in GNSS denied environments—part 1," *Inside GNSS Magazine*, pp. 56–64., May 2019.
- [23] Z. Kassas, J. Morales, and J. Khalife, "New-age satellitebased navigation – STAN: simultaneous tracking and navigation with LEO satellite signals," *Inside GNSS Magazine*, vol. 14, no. 4, pp. 56–65, 2019.
- [24] T. Reid, "Orbital diversity of global navigation satellite systems," Ph.D. dissertation, Stanford University, USA, 2017.
- [25] D. Lawrence, H. Cobb, G. Gutt, M. O'Connor, T. Reid, T. Walter, and D. Whelan, "Navigation from LEO: Current capability and future promise," *GPS World Magazine*, vol. 28, no. 7, pp. 42–48, July 2017.
- [26] D. Lawrence, H. Cobb, G. Gutt, F. Tremblay, P. Laplante, and M. O'Connor, "Test results from a LEO-satellite-based assured time and location solution," in *Proceedings of ION International Technical Meeting Conference*, January 2016, pp. 125–129.
- [27] J. Morales, J. Khalife, A. Abdallah, C. Ardito, and Z. Kassas, "Inertial navigation system aiding with Orbcomm LEO satellite Doppler measurements," in *Proceedings of ION GNSS Conference*, September 2018, pp. 2718–2725.
- [28] J. Morales and Z. Kassas, "A low communication rate distributed inertial navigation architecture with cellular signal aiding," in *Proceedings of IEEE Vehicular Technology Conference*, 2018, pp. 1–6.
- [29] C. Ardito, J. Morales, J. Khalife, A. Abdallah, and Z. Kassas, "Performance evaluation of navigation using LEO satellite signals with periodically transmitted satellite positions," in *Proceedings of ION International Technical Meeting Conference*, 2019, accepted.
- [30] J. Morales and Z. Kassas, "Distributed signals of opportunity aided inertial navigation with intermittent communication," in *Proceedings of ION GNSS Conference*, September 2017, pp. 2519–2530.
- [31] J. Morales and Z. Kassas, "Information fusion strategies for collaborative radio SLAM," in *Proceedings of IEEE/ION Position Location and Navigation Symposium*, April 2018, pp. 1445–1454.
- [32] J. Morales, J. Khalife, and Z. Kassas, "Simultaneous tracking of Orbcomm LEO satellites and inertial navigation system aiding using Doppler measurements," in *Proceedings of IEEE Vehicular Technology Conference*, April 2019, pp. 1–6.
- [33] D. Gebre-Egziabher, "What is the difference between 'loose', 'tight', 'ultra-tight' and 'deep' integration strategies for INS and GNSS," *Inside GNSS*, pp. 28–33, January 2007.
- [34] J. Farrell and M. Barth, *The Global Positioning System and Inertial Navigation*. New York: McGraw-Hill, 1998.
- [35] Z. Kassas and T. Humphreys, "Observability analysis of collaborative opportunistic navigation with pseudorange measurements," *IEEE Transactions on Intelligent Transportation Systems*, vol. 15, no. 1, pp. 260–273, February 2014.
- [36] P. Misra and P. Enge, *Global Positioning System: Signals, Measurements, and Performance*, 2nd ed. Ganga-Jamuna Press, 2010.
- [37] Orbcomm, <https://www.orbcomm.com/en/networks/satellite>, accessed September 30, 2018.
- [38] North American Aerospace Defense Command (NORAD), "Two-line element sets," <http://celestrak.com/NORAD/elements/>.
- [39] D. Vallado and P. Crawford, "SGP4 orbit determination," in *Proceedings of AIAA/AAS Astrodynamics Specialist Conference and Exhibit*, August 2008.
- [40] J. Vetter, "Fifty years of orbit determination: Development of modern astrodynamics methods," *Johns Hopkins APL Technical Digest*, vol. 27, no. 3, pp. 239–252, November 2007.
- [41] B. Tapley, M. Watkins, C. Ries, W. Davis, R. Eanes, S. Poole, H. Rim, B. Schutz, C. Shum, R. Nerem, F. Lerch, J. Marshall, S. Klosko, N. Pavlis, and R. Williamson, "The joint gravity model 3," *Journal of Geophysical Research*, vol. 101, no. B12, pp. 28 029–28 049., December 1996.
- [42] J. Vinti, *Orbital and Celestial Mechanics*. American Institute of Aeronautics and Astronautics, 1998.
- [43] J. Khalife and Z. Kassas, "Receiver design for Doppler positioning with LEO satellites," in *Proceedings of IEEE International Conference on Acoustics, Speech and Signal Processing*, May 2019, pp. 5506–5510.